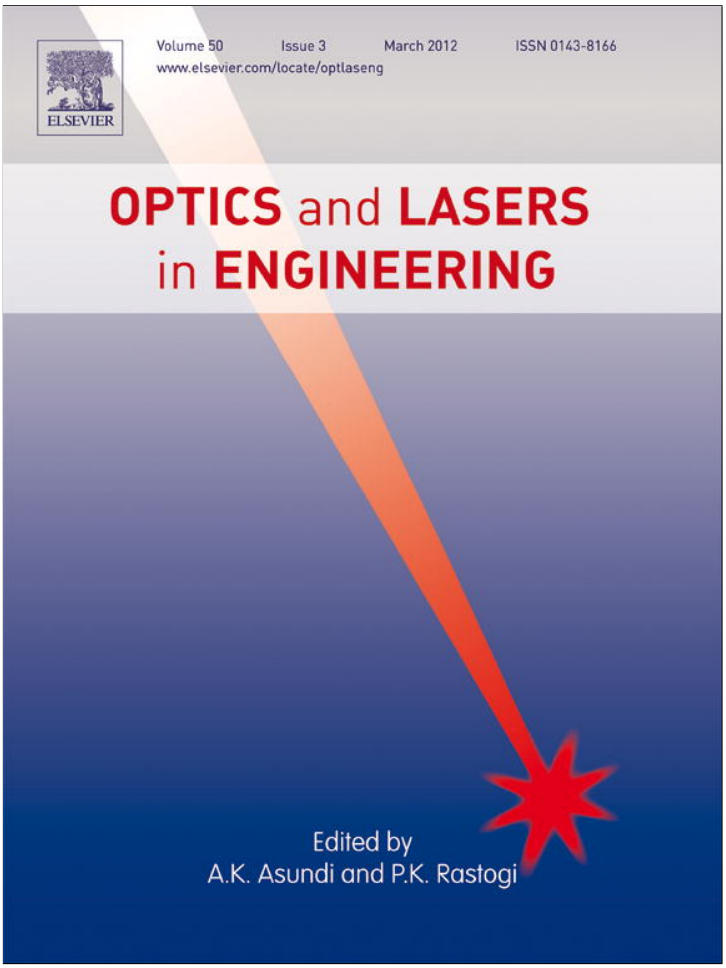

Optics and Lasers in Engineering 50 (2012) 496–501

Contents lists available at SciVerse ScienceDirect

Optics and Lasers in Engineering

journal homepage: www.elsevier.com/locate/optlaseng

Polynomial approximation method for tomographic reconstruction of three-dimensional refractive index fields with limited data

Chao Tian, Yongying Yang *, Yongmo Zhuo, Tong Ling, Haoran Li

State Key Laboratory of Modern Optical Instrumentation, Zhejiang University, 38 Zheda Road, Hangzhou 310027, China

ARTICLE INFO

Article history:
Received 21 February 2011
Received in revised form
9 June 2011
Accepted 27 September 2011
Available online 3 November 2011

Keywords:
Interferometry
Tomography
Flow visualization
Refractive index fields reconstruction

ABSTRACT

We propose a polynomial approximation method (PAM) for reconstruction of three-dimensional refractive index fields by interferometric tomography using limited data. Based on the assumption that the fields to be reconstructed are usually smooth and can be decomposed into a finite order of (orthogonal) polynomials, a set of linear equations can be constructed using both the measured projection data and the Radon transform of the basis functions. By solving these equations, the least-squares solutions of expansion coefficients can be obtained and then substituted back to yield the desired fields. Numerical results have demonstrated that the proposed method is fast, robust to noise and can achieve satisfactory results for refractive index fields with limited projection views and large opaque objects.

1. Introduction

Interferometric tomography has been demonstrated to be a powerful diagnostic technique for high-speed aerodynamic flows due to its advantages of nonintrusive and instantaneous measurement [1–7]. In this technique, interferometers [8,9] such as Mach–Zehnder interferometer or holographic interferometer are usually employed to record multidirectional interferograms that are phase modulated by the changes in optical pathlength of the rays passing through the flow fields. Extracting the phase information from the recorded interferograms [10–13], the projection data can be obtained and thus used for three-dimensional refractive index fields reconstruction.

To reconstruct a three-dimensional refractive index field $f(x,y,z)$, it is convenient to consider the reconstruction of its arbitrary two-dimensional slice $f(x,y)$. In interferometry, the optical pathlength $g(s,\theta)$ of a ray inclined at angle θ from the y-axis and at a distance s from the origin (Fig. 1) can be written as

$$g(s,\theta)=\int_l f(x,y)dl \tag{1}$$

where $f(x,y)=n(x,y)-n_0$ is the difference between the field $n(x,y)$ to be measured and its reference n_0 and the integral is evaluated along the ray path l. In general, the rays that pass through the refractive index field will be refracted and travel in curved lines. However, for weakly refracting fields, the effect is minor and can be neglected [2]. In this way, Eq. (1) may be directly considered as the Radon transform (RT) [14] of the field $f(x,y)$, which is the mathematical foundation of Computed Tomography (CT).

Generally, tomographic reconstruction of the field $f(x,y)$ can be realized if the inverse Radon transform (IRT) of Eq. (1) is solvable. Provided with enough projection views evenly spaced from 0° to 180°, the IRT can be obtained using standard algorithms [14]. However, in interferometric tomography, the number of views is usually limited and the projection data of each view is probably incomplete due to constraints of the enclosures and opaque objects, which we call limited-data situations. For these cases, reconstruction of the field $f(x,y)$ from limited data that is mathematically ill-posed is required.

Tomographic reconstruction methods for limited-data situations generally fall into two groups, namely, analytical reconstruction methods and algebraic reconstruction methods [14]. The analytical reconstruction methods that are based on the direct inversion formula of the Radon transform are fast and computationally efficient but require a large number of projections. For incomplete projection cases, the missing data usually needs to be estimated first using certain interpolation techniques before standard reconstruction [15]. The algebraic reconstruction methods, for example algebraic reconstruction technique (ART) [16] and its improved version simultaneous iterative reconstruction technique (SIRT) [1], which solve a set of equations using an iterative scheme require fewer projection views and can deal with incomplete-data cases but lack accuracy and speed of implementation.

In the past few decades, many techniques have been proposed to deal with limited-data situations [17–21]. Choi et al. considered the data-missing problem due to opaque obstructions in ultrasonic

* Corresponding author. Tel./fax: +86 571 87951514.
E-mail addresses: chaotian02@gmail.com (C. Tian), chuyyy@zju.edu.cn (Y. Yang).

0143-8166/$ - see front matter © 2011 Elsevier Ltd. All rights reserved.
doi:10.1016/j.optlaseng.2011.09.013

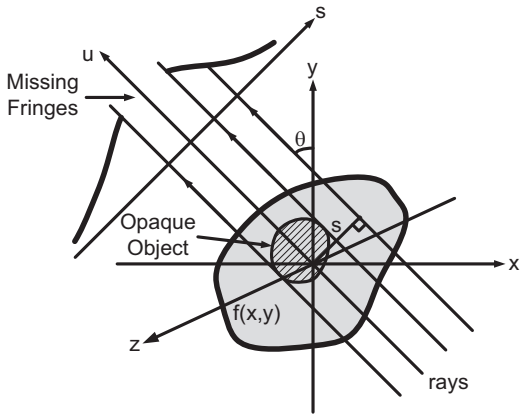

Fig. 1. Projection of a field with an opaque object inside.

CT and proposed an iterative modification scheme for reconstruction [22]. Medoff et al. derived iterative convolution backprojection algorithms and used a priori information to reduce streak artifacts of the results [15]. Cha et al. proposed a complementary field method for ill-posed interferometric tomography problem, which is based on the iterative reconstruction of the difference between the real field and its estimate [23,24]. Later Verhoeven discussed a variety of tomographic algorithms and concluded that the multiplicative algebraic reconstruction techniques (MART) gave the best results for limited-data reconstruction [25,26]. More recently, Song et al. successfully reconstructed density field in a hypersonic wind tunnel using a modified ART method [27] and Mishra et al. evaluated various algebraic methods (i.e. ART, MART) for incomplete-data reconstruction [28].

In this paper, we propose a polynomial approximation method (PAM) for tomographic reconstruction of three-dimensional refractive index fields from limited projection data. The proposed method is simple, fast, robust to noise and can accurately reconstruct refractive index fields with limited number of projection views and large opaque regions.

The organization of the paper is as follows: In Section 2 we introduce the proposed method; in Section 3 we present some discussions and numerical experiments that illustrate its performance; and in Section 4 we draw some conclusions.

2. Polynomial approximation method

Suppose the original two-dimensional field $f(x,y)$ is continuous and smooth [23] and to find an approximation function $\hat{f}(x,y)$ of it, we should try to minimize the residual function $f(x,y)-\hat{f}(x,y)$, that is,

$$\min_{\hat{f}(x,y)} \|f(x,y)-\hat{f}(x,y)\|_2, \tag{2}$$

where $\|\cdot\|_2$ represents the Euclidean norm and $\min_{\hat{f}(x,y)}$ means to find a solution $\hat{f}(x,y)$ that minimizes the norm. Conveniently, the approximation function $\hat{f}(x,y)$ can be written as a linear combination of N degrees of freedom of independent polynomials up to an order n, i.e.,

$$f(x,y) \cong \hat{f}(x,y) = \sum_{j=0}^{N-1} \psi_j(x,y)c_j, \tag{3}$$

where c_j is the expansion coefficient of the basis function $\psi_j(x,y)$ whose order is no greater than n.

In general, the problem in Eq. (2) can be solved by least-squares methods using discrete data of the original field $f(x,y)$. However, what we measured in interferometric tomography is the projection data of the field $f(x,y)$ rather than its own. As a result, some modifications are needed to solve the problem.

Doing Radon transform on both sides of Eq. (3), we get

$$g(s,\theta) = \mathcal{R}[f(x,y)] \cong \mathcal{R}[\hat{f}(x,y)] = \mathcal{R}\left[\sum_{j=0}^{N-1} \psi_j(x,y)c_j\right], \tag{4}$$

where $\mathcal{R}[\cdot]$ is the Radon transform operator defined in Eq. (1). Without considering the approximation error in Eq. (3) and using the linearity property of the Radon transform [14], Eq. (4) can be written in the following form:

$$\sum_{j=0}^{N-1} \Psi_j(s,\theta)c_j = g(s,\theta), \tag{5}$$

where $\Psi_j(s,\theta) = \text{realine}[\psi_j(x,y)]$

To determine the expansion coefficients in Eq. (5), discrete approximations of the Radon transform of the basis functions are needed. One simple and commonly used approach is to first discretize the field $f(x,y)$ into square grids with width δ and then use a ray-tracing strategy in the refractiveless limit to calculate projection matrices ω whose elements are the contributions of the grids to the ray integrals [2,14], as shown in Fig. 2. Accordingly, the discrete version of Eq. (5) can be written as:

$$\sum_{j=0}^{N-1}\sum_{k=1}^{K} \omega_{mk}\psi_{jk}c_j = g_m, \quad m = 1,2,\ldots,M, \tag{6}$$

where M is the total number of rays for all views, K is the number of grids, ω_{mk} is the length of the mth ray in the kth grid and ψ_{jk} is the value of the basis function ψ_j in the kth grid. It should be noted that the missing rays on the detector are not considered in Eq. (6).

Defining $\Psi = \omega\psi$, Eq. (6) can be rewritten in the familiar matrix form:

$$\mathbf{\Psi c} = \mathbf{g}, \tag{7}$$

where

$$\mathbf{c} = \begin{bmatrix} c_0 & c_1 & \cdots & c_{N-1} \end{bmatrix}^T \in \mathbb{R}^{N\times 1}$$

$$\mathbf{g} = \begin{bmatrix} g_1 & g_2 & \cdots & g_M \end{bmatrix}^T \in \mathbb{R}^{M\times 1}$$

$$\mathbf{\Psi} = \begin{bmatrix} \Psi_{1,0} & \Psi_{1,1} & \cdots & \Psi_{1,N-1} \\ \Psi_{2,0} & \Psi_{2,1} & \cdots & \Psi_{2,N-1} \\ \vdots & \vdots & \cdots & \vdots \\ \Psi_{M,0} & \Psi_{M,1} & \cdots & \Psi_{M,N-1} \end{bmatrix} \in \mathbb{R}^{M\times N}$$

and its element $\Psi_{mj} = \omega_m\psi_j = \sum_{k=1}^{K} \omega_{mk}\psi_{jk}$.

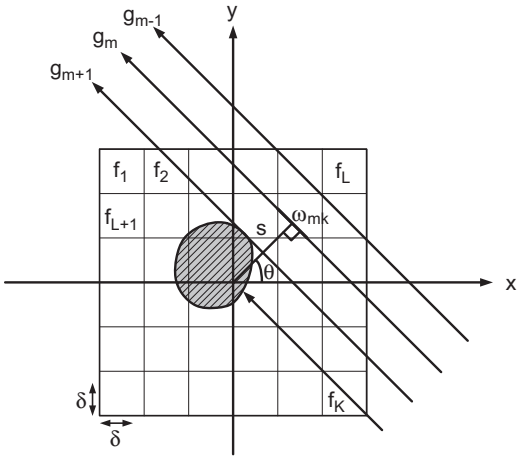

Fig. 2. Ray-tracing scheme for discrete approximations of the Radon transform. See the text for details.

In practice, Eq. (7) is overdetermined (i.e., more equations M than the unknowns N) and ill-posed (due to the limited-data nature of interferometric tomography) and has no exact solutions. However, this does not mean that it can not be evaluated for a meaningful solution. Similar to Eq. (2), we may find some suitable solutions $\mathbf{c}$ that give the best fit to the unknown filed $f(x,y)$ by minimize the following least-squares residual; that is

$$\min_{\mathbf{c}} \|\mathbf{\Psi}c-\mathbf{g}\|_2. \tag{8}$$

Ordinarily, the normal equations method can be directly applied to determine the expansion coefficients $\mathbf{c}$ [29]. However, it is not preferred because of its instability for ill-posed problems. Therefore, we use the truncated singular value decomposition (TSVD) method as an alternative [26]. Mathematically, the SVD of the coefficient matrix $\mathbf{\Psi}$ can be represented as

$$\mathbf{\Psi} = U\mathbf{\Sigma}\mathbf{V}^T, \tag{9}$$

where $\mathbf{U}\in\mathbb{R}^{M\times M}$ as well as $\mathbf{V}\in\mathbb{R}^{N\times N}$ are both orthogonal matrices and $\mathbf{\Sigma}\in\mathbb{R}^{M\times N}$ is a diagonal matrix whose diagonal elements σ are the singular values. According to Eqs. (7) and (9), the expansion coefficients can be computed directly from the SVD

$$\mathbf{c} = \mathbf{V}\mathbf{\Sigma}^{+}\mathbf{U}^T\mathbf{g}, \tag{10}$$

where $\mathbf{\Sigma}^{+}\in\mathbb{R}^{N\times M}$ is the pseudoinverse of the matrix $\mathbf{\Sigma}$ and its diagonal elements σ^{+} are defined as

$$\sigma_i{}^{+} = \begin{cases} 1/\sigma_i, & \text{when } \sigma_i > \tau\sigma_{\max} \\ 0, & \text{else} \end{cases}, \tag{11}$$

where $i=1,2,\ldots,\min(M,N)$, $\sigma_{\max}$ is the maximum singular values of the coefficient matrix $\mathbf{\Psi}$ and τ is a truncation parameter that controls error.

Once the coefficients are calculated using Eq. (10), they may be immediately substituted into Eq. (3) to yield an estimate of the true field $f(x,y)$. In this way, we call it the polynomial approximation method (PAM) for tomographic reconstruction with limited data. Applying the PAM to other slices along the z-axis, the three-dimensional refractive fields $f(x,y,z)$ can be finally reconstructed.

It should be noted that the two-dimensional approximation function $\hat{f}(x,y)$ (Eq. (3)) can be a combination of any kind of polynomial in theory. However, it is not so in practice. For instance, if higher-order power series are employed as the basis functions, the coefficient matrix $\mathbf{\Psi}$ will be so ill-conditioned that no valid solutions can be expected. In fact, this is an extremely unstable process because the coefficient matrix $\mathbf{\Psi}$ is related to the famous Hilbert matrix, which is a classical example of ill-conditioned matrix [30].

To overcome this difficulty, orthogonal polynomials such as Zernike polynomials, Chebyshev polynomials and Legendre polynomials that can cure the ill-conditioning of the coefficient matrix $\mathbf{\Psi}$ are recommended in the PAM. As a matter of fact, the Zernike polynomials [31,32] that are orthogonal on a unit disk were used as the basis functions in all the examples presented below. When written in polar coordinates as products of angular functions and radial polynomials, they can be formulated as

$$\left.\begin{array}{l} Z_{\text{even } j} = [2(n+1)]^{1/2}R_n^m(\rho)\cos m\theta \\ Z_{\text{odd } j} = [2(n+1)]^{1/2}R_n^m(\rho)\sin m\theta \end{array}\right\} \quad m\neq 0 \\ Z_j = [(n+1)]^{1/2}R_n^m(\rho) \quad m=0 \Bigg\} \tag{12}$$

where $j=1,2,\ldots,N$ is a mode ordering number and

$$R_n^m(\rho) = \sum_{s=0}^{(n-m)/2} \frac{(-1)^s(n-s)!}{s![(n+m)/2-s]![(n-m)/2-s]!}\rho^{n-2s} \tag{13}$$

where the indices n and m are radial degree and the azimuthal frequency, respectively, and satisfy $m\le n$, $n-|m|=$even. The degrees of freedom $N=(n+1)(n+2)/2$.

3. Discussion and numerical results

From the above process, one may find that the proposed PAM is similar to the well-known ART and its improvement SIRT. However, they differ in two aspects at least. First the PAM employs global functions [i.e., $\psi_j(x,y)$] as the basis of approximation while the ART uses a local basis (i.e., pixel basis) [16,33]. For this reason, the reconstructed images by use of the PAM usually look smoother than those by the ART (see the examples below). Second since the PAM has much fewer degrees of freedom (i.e., unknowns) to be determined than the ART, therefore the size of the coefficient matrix $\mathbf{\Psi}$ of the PAM is much smaller, which makes it possible to use noniterative techniques to achieve faster computation. To illustrate this difference, suppose a field $f(x,y)$ is discretized into 256×256 grids. If 256 projection rays in each of 10 projection views passing through the field are acquired (note that $M=2560$) and 15 orders of orthogonal polynomials are used as the basis functions, the degrees of freedom $N=136$ (see Section 2) and the size of the coefficient matrix $\mathbf{\Psi}$ is 2560×136. In contrast, under the same conditions, the number of unknowns to be estimated in the ART equals the grids number ($N=65{,}536$) and hence the size of the matrix $\mathbf{\Psi}$ is $2560\times 65{,}536$, which is 480 times bigger than that in the PAM. Note also that the equations in the PAM are usually overdetermined ($2560>136$) whereas those in the ART are underdetermined ($2560<65536$) and this contrast becomes more obvious for limited-data situations in interferometric tomography.

To verify the performance of the proposed PAM, we used a synthetic function $f(x,y)$ with 256×256 pixels to simulate a relative refractive index field (Fig. 3(a)) and compared the reconstruction results of the PAM with those of the classical simultaneous iterative reconstruction technique (SIRT) [1]. Specifically, the function $f(x,y)$ has the following form:

$$\begin{aligned} f(x,y) = 0.03\times\{&3(1-x)^2\exp[-x^2-(y+1)^2] \\ &-10(x/5-x^3-y^5)\exp(-x^2-y^2) \\ &-1/3\exp[-(x+1)^2-y^2]\}\times \text{mask} \end{aligned} \tag{14}$$

where $-3\le x,y\le 3$ and mask is a circular aperture that equals 1 if inside the pupil and 0 otherwise. Since $f(x,y)$ is a dimensionless quantity (i.e., relative refractive index), the unit in some of the figures below is not given. Note also that a truncation parameter $\tau=0.04$ was used throughout the following experiments.

Fig. 3 shows that the synthetic field $f(x,y)$ was successfully reconstructed by use of the PAM from noiseless projections data. The projection matrix g as well as the coefficient matrix $\mathbf{\Psi}$ (Eq. (7)) was generated from 10 equally spaced views covering the entire angle of 180° with 256 rays each. Here 15 orders of Zernike polynomials were employed to approximate the unknown field and the estimated 231 expansion coefficients are illustrated in Fig. 3(b). As we can see, the values of these coefficients become smaller with the increase of the mode number j, which means that high-frequency basis functions make little contribution to the estimated field and thus can be discarded within tolerance. Fig. 3(c) and (d) shows the reconstructed field using the estimated coefficients and the profiles of the true field and its estimate in row 100, respectively. Note how close they are except small edge distortions.

It should be noted that the reconstruction results of the PAM depend on the value of the expansion order n due to the fact that low-order expansions of complex fields and higher-order expansions of simple fields are both inappropriate. Some empirical studies were performed to verify how its values influence the final reconstruction results. For the same field in Fig. 3(a), different orders (ranging from 8 to 20) of Zernike polynomials were used to perform the approximations under the same

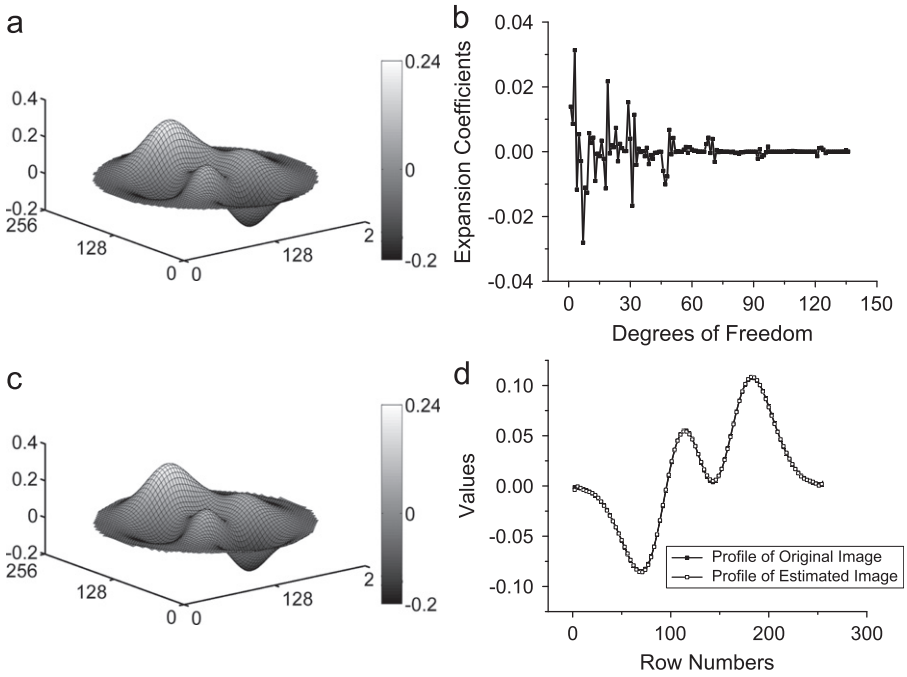

Fig. 3. Reconstruction of the field $f(x,y)$ using noiseless projection data by the PAM: (a) synthetic field $f(x,y)$, (b) estimated expansion coefficients $\mathbf{c}$, (c) reconstructed field $\hat{f}(x,y)$ using the coefficients in (b), (d) profiles of (a) and (c) in row 100. Note that figures (a) and (c) are plotted in the same scale.

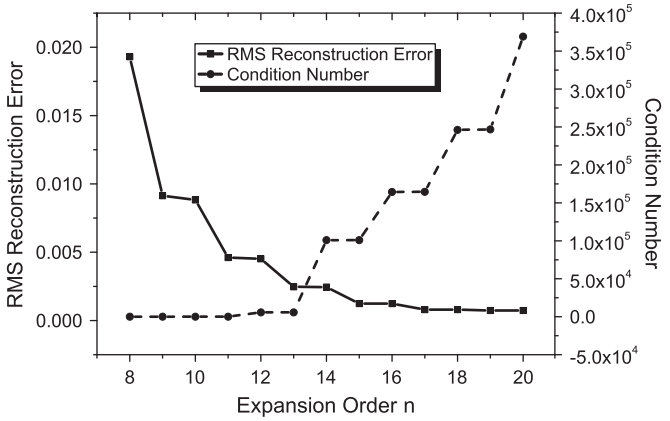

Fig. 4. RMS reconstruction errors and condition numbers of the coefficient matrix $\mathbf{\Psi}$ versus the expansion order n.

conditions as the previous example (Fig. 3) and Fig. 4 shows the change of the root mean squares (RMS) reconstruction errors versus the expansion order n, which are calculated as

$$\text{error}_{\text{rms}} = \frac{1}{V}\sum_{V}(f-\hat{f})^2 \tag{15}$$

where V is the number of valid data. We can see that the RMS reconstruction errors decline rapidly with the increase of the value of the order n. Until here, one may think that more accurate approximations of the desired field can be obtained provided the expansion order n is high enough. However, as the ill-conditioning of the matrix $\mathbf{\Psi}$ grows worse rapidly with the increase of the value of the order n (Fig. 4), the expansion coefficient $\mathbf{c}$ will be highly susceptible to noise. In other words, a moderate order n that makes a compromise between the reconstruction accuracy and robustness will be appreciated.

Fig. 5 shows the noise suppression ability of the proposed method. The same 10 projection data was generated as before (Fig. 3) but corrupted with uniformly distributed noise with amplitude of $\pm 5\%$ of the maximum projection value, which results in a signal-to-noise ration of about 18 dB. The noisy and true projections of the view $\theta = 36^\circ$ are shown in Fig. 5(a). Ten orders of Zernike polynomials were utilized to approximate the unknown field and the estimated 66 coefficients as well as the reconstructed field are shown in Fig. 5(b) and (c), respectively. Fig. 5(d) is the difference between the reconstructed(Fig. 5(c)) and the original field (Fig. 3(a)). Note the similarity of the first 66 coefficients between Figs. 5(b) and 3(b). From this experiment, we can see that the PAM can give satisfactory results with limited projection views and noisy data.

Finally, to investigate the performance of the PAM for the cases with missing projection data, we also simulated an incomplete field by use of the same field $f(x,y)$ in Fig. 3(a) except a circular opaque object with radius $r = 0.4r_{\max}$ in the center, where $r_{\max}$ is the maximum radius of the valid data. With the same degrees of freedom of Zernike polynomials, projection views and amount of noise as in the previous example (Fig. 5), the finally reconstructed field and its deviation from the true field are shown in Fig. 6(a) and (b), respectively, from which we can see that the proposed PAM is also effective for incomplete-data cases.

For comparison, we reconstructed the same incomplete field under identical conditions (Fig. 5(a)) with the PAM using the SIRT in Ref. [1] and showed the reconstructed field as well as the error in Fig. 6(c) and (d), separately. The total number of iterations and relaxation factor used for the SIRT were 5000 and 0.3, respectively. From Fig. 6(c) and (d), we may find that the SIRT suffered from noise, yielded less smooth images and could only give a coarse shape of the original field. Note that the rays passing through the opaque region were neglected for both the SIRT and PAM and the total time used by them was 205.9 and 42.4 s, respectively, based on a computer with Core 2 Duo CPU of 2.1 GHz main frequency using Matlab.

4. Conclusion

We present a polynomial approximation method (PAM) for tomographic reconstruction of refractive index fields using limited

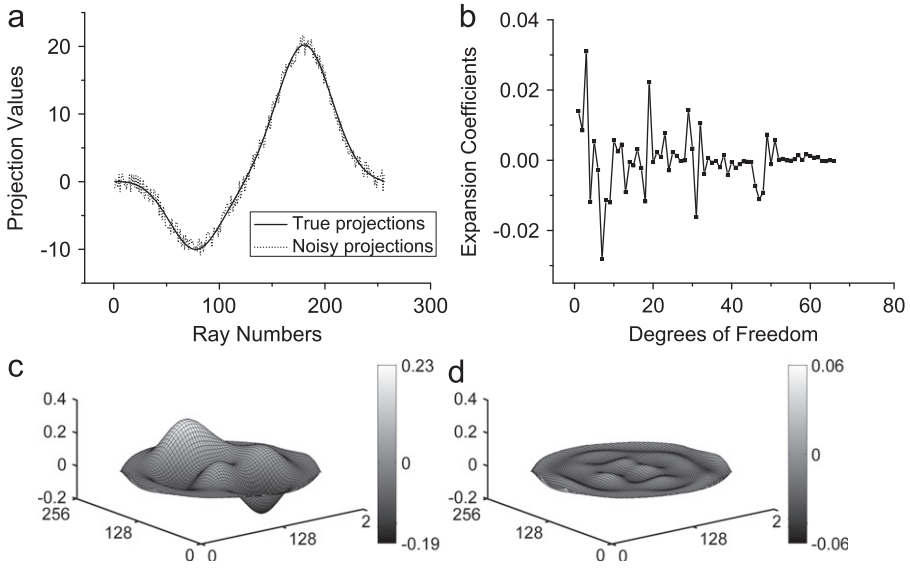

Fig. 5. Reconstruction of the field in Fig. 3(a) using noisy projection data by the PAM: (a) true projections (solid line) and noisy projections (dotted line) of the view $\theta=36^{\circ}$, (b) estimated expansion coefficients $\mathbf{c}$, (c) recovered field $\hat{f}(x,y)$ using the coefficients in (b), (d) difference between (c) and the original field (Fig. 3(a)). Note the similarity of the first 66 coefficients between Figs. 5(b) and 3(b).

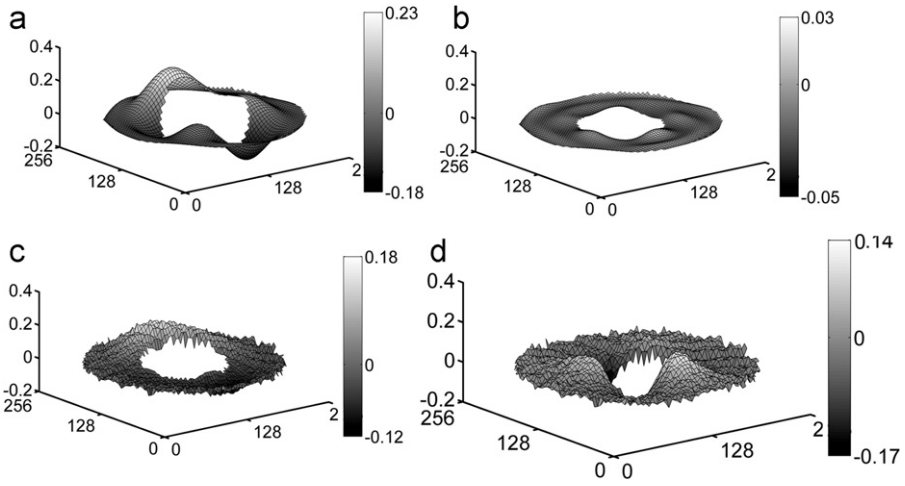

Fig. 6. Reconstruction of the field $f(x,y)$ with a hole in the center from noisy projection data: (a) and (c) reconstructed fields by the PAM and SIRT, respectively; (b) and (d) error fields of (a) and (c), respectively.

interferometric projection data. In this method, we use a finite order of orthogonal polynomials to approximate the original fields, construct a set of simultaneous equations using Radon transform, then estimate the least-squares expansion coefficients from the overdetermined system and finally reconstruct the field. This is reasonable and can achieve satisfactory results as long as the smoothness assumption of the original field holds. The reason that why orthogonal polynomials (instead of non-orthogonal ones) are chosen as the basis functions is due to the fact that they generally have less redundancy and can improve the behavior of the coefficient matrix $\mathbf{\Psi}$. Moreover, the TSVD method that can give stable numerical results is utilized to help to deal with the ill-conditioning of the problem.

Since the proposed PAM uses global polynomials [i.e., $\psi_j(x,y)$] as the basis functions, it generally has much fewer unknowns and can be directly implemented using noniterative methods compared with the classical ART. Meanwhile, this also makes it robust to noise, insensitive to data-missing cases and yield smoother images, as shown in Figs. 5 and 6. For refractive index fields with simpler shapes, which are the typical situations in experiments, the proposed method is promised to give more accurate results.

Acknowledgments

This work was supported by the Aerospace Innovation Fund of China Aerospace Science and Technology Corporation (CASC) under grant 2009200054, the Key Programs of the State Key Laboratory of Modern Optical Instrumentation, Zhejiang University and the Scholarship Award for Excellent Doctoral Student granted by Ministry of Education.

References

[1] Gilbert P. Iterative methods for the three-dimensional reconstruction of an object from projections. J Theor Biol 1972;36:105–17.
[2] Sweeney DW, Vest CM. Reconstruction of three-dimensional refractive index fields from multidirectional interferometric data. Appl Opt 1973;12:2649–64.
[3] Matulka RD, Collins DJ. Determination of three-dimensional density fields from holographic interferograms. J Appl Phys 1971;42:1109–19.
[4] Hertz HM. Experimental determination of 2-D flame temperature fields by interferometric tomography. Opt Commun 1985;54:131–6.
[5] Wang D, Zhuang T. The measurement of 3-D asymmetric temperature field by using real time laser interferometric tomography. Opt Lasers Eng 2001;36:289–97.

[6] Fomin N, Lavinskaya E, Takayama K. Limited projections laser speckle tomography of complex flows. Opt Lasers Eng 2006;44:335–49.
[7] Zhang B, He Y, Song Y, He A. Deflection tomographic reconstruction of a complex flow field from incomplete projection data. Opt Lasers Eng 2009;47:1183–8.
[8] Shakher C, Nirala AK. A review on refractive index and temperature profile measurements using laser-based interferometric techniques. Opt Lasers Eng 1999;31:455–91.
[9] Srivastava A, Muralidhar K, Panigrahi PK. Reconstruction of the concentration field around a growing KDP crystal with schlieren tomography. Appl Opt 2005;44:5381–92.
[10] Tian C, Yang Y, Liu D, Luo Y, Zhuo Y. Demodulation of a single complex fringe interferogram with a path-independent regularized phase-tracking technique. Appl Opt 2010;49:170–9.
[11] Tian C, Yang Y, Zhang S, Liu D, Luo Y, Zhuo Y. Regularized frequency-stabilizing method for single closed-fringe interferogram demodulation. Opt Lett 2010;35:1837–9.
[12] Mishra D, Muralidhar K, Munshi P. Performance evaluation of fringe thinning algorithms for interferometric tomography. Opt Lasers Eng 1998;30:229–49.
[13] Wei Y, Yan D, Stephen Cha S. Comparison of results of interferometric phase extraction algorithms for three-dimensional flow-field tomography. Opt Lasers Eng 1999;32:147–55.
[14] Kak AC, Slaney M. Principles of computerized tomographic imaging. New York: IEEE Press; 1999.
[15] Medoff BP, Brody WR, Nassi M, Macovski A. Iterative convolution back-projection algorithms for image reconstruction from limited data. J Opt Soc Am 1983;73:1493–500.
[16] Gordon R, Bender R, Herman GT. Algebraic reconstruction techniques (ART) for three-dimensional electron microscopy and X-ray photography. J Theor Biol 1970;29:471–81.
[17] Bahl S, Liburdy JA. Three-dimensional image reconstruction using interferometric data from a limited field of view with noise. Appl Opt 1991;30:4218–26.
[18] Subbarao PMV, Munshi P, Muralidhar K. Performance evaluation of iterative tomographic algorithms applied to reconstruction of a three-dimensional temperature field. Numer Heat Transfer Part B—Fundam 1997;31:347–72.
[19] Kihm KD, Lyons DP. Optical tomography using a genetic algorithm. Opt Lett 1996;21:1327–9.
[20] Zhang Y, Ruff GA. Three-dimensional temperature measurements in enclosures by using multiview interferometric tomography. Meas Sci Technol 1994;5:495.
[21] Subbarao PMV, Munshi P, Muralidhar K. Performance of iterative tomographic algorithms applied to non-destructive evaluation with limited data. Ndt & E Int 1997;30:359–70.
[22] Choi JS, Ogawa K, Nakajima M, Yuta S. A reconstruction algorithm of body sections with opaque obstructions, sonics and ultrasonics. IEEE Trans 1982;29:143–50.
[23] Cha SS, Sun H. Tomography for reconstructing continuous fields from ill-posed multidirectional interferometric data. Appl Opt 1990;29:251–8.
[24] Cha DJ, Chat SS. Variable grid decomposition for ill-posed interferometric tomography: comparison of algorithms. Opt Lasers Eng 1997;28:181–97.
[25] Verhoeven DD. Multiplicative algebraic computed tomographic algorithms for the reconstruction of multidirectional interferometric data. Opt Eng 1993;32:410–9.
[26] Verhoeven D. Limited-data computed tomography algorithms for the physical sciences. Appl Opt 1993;32:3736–54.
[27] Song Y, Zhang B, He A. Algebraic iterative algorithm for deflection tomography and its application to density flow fields in a hypersonic wind tunnel. Appl Opt 2006;45:8092–101.
[28] Mishra D, Longtin JP, Singh RP, Prasad V. Performance evaluation of iterative tomography algorithms for incomplete projection data. Appl Opt 2004;43:1522–32.
[29] Golub. Matrix computation. 3rd ed. London: The Johns Hopkins University Press; 1996.
[30] Burden RL, Faires JD. Numerical analysis. 7th ed.Brooks Cole; 2001.
[31] Noll RJ. Zernike polynomials and atmospheric turbulence. J Opt Soc Am 1976;66:207–11.
[32] Wang JY, Silva DE. Wave-front interpretation with Zernike polynomials. Appl Opt 1980;19:1510–8.
[33] Andersen AH, Kak AC. Simultaneous algebraic reconstruction technique (SART): a superior implementation of the ART algorithm. Ultrason Imaging 1984;6:81–94.